Eur. Phys. J. C (2013) 73:2531
DOI 10.1140/epjc/s10052-013-2531-6

THE EUROPEAN PHYSICAL JOURNAL C

Regular Article - Experimental Physics

Hadron transverse momentum distributions in muon deep inelastic scattering at 160 GeV/*c*

C. Adolph[8], M.G. Alekseev[24], V.Yu. Alexakhin[7], Yu. Alexandrov[15,b], G.D. Alexeev[7], A. Amoroso[27], V. Andrieux[22], A. Austregesilo[10,17], B. Badełek[32], F. Balestra[27], J. Barth[4], G. Baum[1], Y. Bedfer[22], A. Berlin[2], J. Bernhard[13], R. Bertini[27], K. Bicker[10,17], J. Bieling[4], R. Birsa[24], J. Bisplinghoff[3], M. Boer[22], P. Bordalo[12,c], F. Bradamante[25], C. Braun[8], A. Bravar[24], A. Bressan[25,a], M. Büchele[9], E. Burtin[22], L. Capozza[22], M. Chiosso[27], S.U. Chung[17], A. Cicuttin[26], M.L. Crespo[26], S. Dalla Torre[24], S.S. Dasgupta[24], S. Dasgupta[6], O.Yu. Denisov[28], S.V. Donskov[21], N. Doshita[34], V. Duic[25], W. Dünnweber[16], M. Dziewiecki[33], A. Efremov[7], C. Elia[25], P.D. Eversheim[3], W. Eyrich[8], M. Faessler[16], A. Ferrero[22], A. Filin[21], M. Finger[19], M. Finger Jr.[19], H. Fischer[9], C. Franco[12], N. du Fresne von Hohenesche[10,13], J.M. Friedrich[17], V. Frolov[10], R. Garfagnini[27], F. Gautheron[2], O.P. Gavrichtchouk[7], S. Gerassimov[15,17], R. Geyer[16], M. Giorgi[25], I. Gnesi[27], B. Gobbo[24], S. Goertz[4], S. Grabmüller[17], A. Grasso[27], B. Grube[17], R. Gushterski[7], A. Guskov[7], T. Guthörl[9,d], F. Haas[17], D. von Harrach[13], F.H. Heinsius[9], F. Herrmann[9], C. Heß[2], F. Hinterberger[3], Ch. Höppner[17], N. Horikawa[18,e], N. d'Hose[22], S. Huber[17], S. Ishimoto[34,f], Yu. Ivanshin[7], T. Iwata[34], R. Jahn[3], V. Jary[20], P. Jasinski[13], R. Joosten[3], E. Kabuß[13], D. Kang[13], B. Ketzer[17], G.V. Khaustov[21], Yu.A. Khokhlov[21,g], Yu. Kisselev[2], F. Klein[4], K. Klimaszewski[31], J.H. Koivuniemi[2], V.N. Kolosov[21], K. Kondo[34], K. Königsmann[9], I. Konorov[15,17], V.F. Konstantinov[21], A.M. Kotzinian[27], O. Kouznetsov[7,22], M. Krämer[17], Z.V. Kroumchtein[7], N. Kuchinski[7], F. Kunne[22], K. Kurek[31], R.P. Kurjata[33], A.A. Lednev[21], A. Lehmann[8], S. Levorato[25], J. Lichtenstadt[23], A. Maggiora[28], A. Magnon[22], N. Makke[22,25], G.K. Mallot[10], A. Mann[17], C. Marchand[22], A. Martin[25], J. Marzec[33], H. Matsuda[34], T. Matsuda[14], G. Meshcheryakov[7], W. Meyer[2], T. Michigami[34], Yu.V. Mikhailov[21], A. Morreale[22,h], A. Nagaytsev[7], T. Nagel[17], F. Nerling[9], S. Neubert[17], D. Neyret[22], V.I. Nikolaenko[21], J. Novy[20], W.-D. Nowak[9], A.S. Nunes[12], A.G. Olshevsky[7], M. Ostrick[13], R. Panknin[4], D. Panzieri[29,30], B. Parsamyan[27], S. Paul[17], G. Piragino[27], S. Platchkov[22], J. Pochodzalla[13], J. Polak[11,25], V.A. Polyakov[21], J. Pretz[4,i], M. Quaresma[12], C. Quintans[12], J.-F. Rajotte[16], S. Ramos[12,c], G. Reicherz[2], E. Rocco[10], V. Rodionov[7], E. Rondio[31], N.S. Rossiyskaya[7], D.I. Ryabchikov[21], V.D. Samoylenko[21], A. Sandacz[31], M.G. Sapozhnikov[7], S. Sarkar[6], I.A. Savin[7], G. Sbrizzai[25], P. Schiavon[25], C. Schill[9], T. Schlüter[16], A. Schmidt[8], K. Schmidt[9,d], L. Schmitt[17,j], H. Schmïden[3], K. Schönning[10], S. Schopferer[9], M. Schott[10], O.Yu. Shevchenko[7], L. Silva[12], L. Sinha[6], S. Sirtl[9], M. Slunecka[19], S. Sosio[27], F. Sozzi[24], A. Srnka[5], L. Steiger[24], M. Stolarski[12], M. Sulc[11], R. Sulej[31], H. Suzuki[34,e], P. Sznajder[31], S. Takekawa[28], J. Ter Wolbeek[9,d], S. Tessaro[24], F. Tessarotto[24], F. Thibaud[22], S. Uhl[17], I. Uman[16], M. Vandenbroucke[22], M. Virius[20], L. Wang[2], T. Weisrock[13], M. Wilfert[13], R. Windmolders[4], W. Wiślicki[31], H. Wollny[22], K. Zaremba[33], M. Zavertyaev[15], E. Zemlyanichkina[7], N. Zhuravlev[7], M. Ziembicki[33]

[1] Fakultät für Physik, Universität Bielefeld, 33501 Bielefeld, Germany[k]
[2] Institut für Experimentalphysik, Universität Bochum, 44780 Bochum, Germany[k]
[3] Helmholtz-Institut für Strahlen- und Kernphysik, Universität Bonn, 53115 Bonn, Germany[k]
[4] Physikalisches Institut, Universität Bonn, 53115 Bonn, Germany[k]
[5] Institute of Scientific Instruments, AS CR, 61264 Brno, Czech Republic[k]
[6] Matrivani Institute of Experimental Research & Education, Calcutta 700 030, India[m]
[7] Joint Institute for Nuclear Research, 141980 Dubna, Moscow region, Russia[n]
[8] Physikalisches Institut, Universität Erlangen–Nürnberg, 91054 Erlangen, Germany[k]
[9] Physikalisches Institut, Universität Freiburg, 79104 Freiburg, Germany[k,r]
[10] CERN, 1211 Geneva 23, Switzerland
[11] Technical University in Liberec, 46117 Liberec, Czech Republic[l]
[12] LIP, 1000-149 Lisbon, Portugal[o]
[13] Institut für Kernphysik, Universität Mainz, 55099 Mainz, Germany[k]
[14] University of Miyazaki, Miyazaki 889-2192, Japan[p]
[15] Lebedev Physical Institute, 119991 Moscow, Russia
[16] Department für Physik, Ludwig-Maximilians-Universität München, 80799 Munich, Germany[k,q]
[17] Physik Department, Technische Universität München, 85748 Garching, Germany[k,q]
[18] Nagoya University, 464 Nagoya, Japan[p]
[19] Faculty of Mathematics and Physics, Charles University in Prague, 18000 Prague, Czech Republic[l]

[20]Czech Technical University in Prague, 16636 Prague, Czech Republic[l,r]
[21]Institute for High Energy Physics, State Research Center of the Russian Federation, 142281 Protvino, Russia
[22]CEA IRFU/SPhN Saclay, 91191 Gif-sur-Yvette, France[r]
[23]School of Physics and Astronomy, Tel Aviv University, 69978 Tel Aviv, Israel[s]
[24]Trieste Section of INFN, 34127 Trieste, Italy
[25]Department of Physics and Trieste Section of INFN, University of Trieste, 34127 Trieste, Italy
[26]Abdus Salam ICTP and Trieste Section of INFN, 34127 Trieste, Italy
[27]Department of Physics and Torino Section of INFN, University of Turin, 10125 Turin, Italy
[28]Torino Section of INFN, 10125 Turin, Italy
[29]University of Eastern Piedmont, 15100 Alessandria, Italy
[30]Torino Section of INFN, 10125 Turin, Italy
[31]National Centre for Nuclear Research, 00-681 Warsaw, Poland[t]
[32]Faculty of Physics, University of Warsaw, 00-681 Warsaw, Poland[t]
[33]Institute of Radioelectronics, Warsaw University of Technology, 00-665 Warsaw, Poland[t]
[34]Yamagata University, Yamagata 992-8510, Japan[p]

Received: 31 May 2013 / Revised: 30 July 2013 / Published online: 23 August 2013

Abstract Multiplicities of charged hadrons produced in deep inelastic muon scattering off a ^{6}LiD target have been measured as a function of the DIS variables x_{Bj}, Q^2, W^2 and the final state hadron variables p_T and z. The p_T^2 distributions are fitted with a single exponential function at low values of p_T^2 to determine the dependence of $\langle p_T^2 \rangle$ on x_{Bj}, Q^2, W^2 and z. The z-dependence of $\langle p_T^2 \rangle$ is shown to be a potential tool to extract the average intrinsic transverse momentum squared of partons, $\langle k_\perp^2 \rangle$, as a function of x_{Bj} and Q^2 in a leading order QCD parton model.

[a] e-mail: Andrea.Bressan@cern.ch

[b]Deceased.

[c]Also at IST, Universidade Técnica de Lisboa, Lisbon, Portugal.

[d]Supported by the DFG Research Training Group Programme 1102 "Physics at Hadron Accelerators".

[e]Also at Chubu University, Kasugai, Aichi, 487-8501 Japan[p].

[f]Also at KEK, 1-1 Oho, Tsukuba, Ibaraki, 305-0801 Japan.

[g]Also at Moscow Institute of Physics and Technology, Moscow Region, 141700, Russia.

[h]Present address: National Science Foundation, 4201 Wilson Boulevard, Arlington, VA 22230, USA.

[i]Present address: RWTH Aachen University, III. Physikalisches Institut, 52056 Aachen, Germany.

[j]Also at GSI mbH, Planckstr. 1, 64291 Darmstadt, Germany.

[k]Supported by the German Bundesministerium für Bildung und Forschung.

[l]Supported by Czech Republic MEYS Grants ME492 and LA242.

[m]Supported by SAIL (CSR), Govt. of India.

[n]Supported by CERN-RFBR Grants 08-02-91009 and 12-02-91500.

[o]Supported by the Portuguese FCT—Fundação para a Ciência e Tecnologia, COMPETE and QREN, Grants CERN/FP/109323/2009, CERN/FP/116376/2010 and CERN/FP/123600/2011.

[p]Supported by the MEXT and the JSPS under the Grants No. 18002006, No. 20540299 and No. 18540281; Daiko Foundation and Yamada Foundation.

[q]Supported by the DFG cluster of excellence 'Origin and Structure of the Universe' (www.universe-cluster.de).

[r]Supported by EU FP7 (HadronPhysics3, Grant Agreement number 283286).

[s]Supported by the Israel Science Foundation, founded by the Israel Academy of Sciences and Humanities.

[t]Supported by the Polish NCN Grant DEC-2011/01/M/ST2/02350.

1 Introduction

Semi-Inclusive measurements of Deep Inelastic Scattering (SIDIS) of leptons off nucleons provide information about the partonic structure of the nucleon and the hadronisation of partons, and hence offer a wide testing ground of Quantum Chromodynamics (QCD). The main subject of the present study are the transverse momentum distributions of charged hadrons produced in the current fragmentation region in lepton-nucleon scattering off unpolarised nucleons. The hadron transverse momentum p_T is defined with respect to the virtual photon direction. The following standard notations are used: ℓ and ℓ' for the incoming and outgoing lepton, N for the target nucleon, h for the outgoing hadron and X for the unobserved particles in the final state; l, l', P, and p denote the 4-momenta of ℓ, ℓ', N, and h. The general expression for the differential SIDIS cross section describing the reaction $\ell + N \to \ell' + h + X$ in the one-photon approximation is [1, 2]:

$$\begin{aligned}\frac{d^5\sigma^h(x_{Bj}, Q^2, z, p_T^2, \phi_h)}{dx_{Bj}\,dQ^2\,dz\,dp_T^2\,d\phi_h} &= \frac{d^4\sigma^h(x_{Bj}, Q^2, z, p_T^2)}{2\pi\,dx_{Bj}\,dQ^2\,dz\,dp_T^2}\big(1 + a_1\big(x_{Bj}, Q^2, z, p_T^2\big)\cos\phi_h \\ &\quad + a_2\big(x_{Bj}, Q^2, z, p_T^2\big)\cos 2\phi_h \\ &\quad + \lambda a_3\big(x_{Bj}, Q^2, z, p_T^2\big)\sin\phi_h\big). \end{aligned} \tag{1}$$

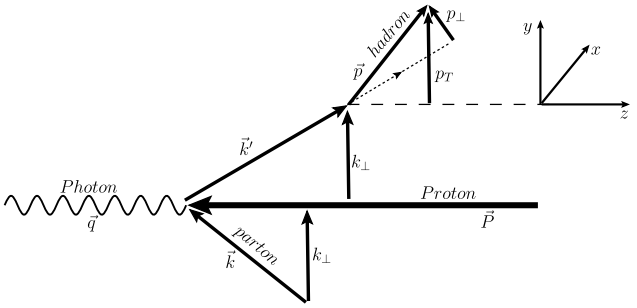

Fig. 1 Sketch showing the kinematic variables for the absorption of a virtual photon by a parton with intrinsic transverse momentum $k_\perp$ and the subsequent hadronisation. The transverse momentum of the observed hadron is denoted by p_T when defined with respect to the virtual photon direction in the photon nucleon center of mass system and by $p_\perp$ when defined with respect to the scattered parton direction

Here, λ is the helicity of the incoming lepton and the standard SIDIS variables are used: the 4-momentum transfer $q = (l - l')$, the photon virtuality $Q^2 = -q^2$, the Bjorken scaling variable $x_{Bj} = Q^2/2P \cdot q$, the hadron fractional energy $z = P \cdot p/P \cdot q$ and the azimuthal angle ϕ_h of the transverse momentum of the hadron with respect to the lepton scattering plane around the virtual photon direction. After integration over ϕ_h, the cross section does not depend on the initial lepton polarisation λ. The hadron multiplicity per interaction is defined as the ratio of the differential SIDIS cross section over the differential DIS cross section $d^2\sigma^{\mathrm{DIS}}(x_{Bj}, Q^2)/dx_{Bj}\,dQ^2$. Thus, the differential hadron multiplicity, $d^2n^h/dz\,dp_T^2$, depends on four variables, x_{Bj}, Q^2, z, p_T^2:

$$\frac{d^2n^h(x_{Bj}, Q^2, z, p_T^2)}{dz\,dp_T^2} = \frac{\frac{d^4\sigma^h(x_{Bj}, Q^2, z, p_T^2)}{dx_{Bj}\,dQ^2\,dz\,dp_T^2}}{\frac{d^2\sigma^{\mathrm{DIS}}(x_{Bj}, Q^2)}{dx_{Bj}\,dQ^2}}. \tag{2}$$

Within a pQCD Leading Order (LO) parton model the shape of the p_T^2 distributions depends on the intrinsic transverse momentum $k_\perp$ of the partons and the transverse momentum of the hadrons $p_\perp$ acquired during parton fragmentation. The amount of the contributions of $k_\perp$ and $p_\perp$ may depend on the hadron type, parton flavour, and on kinematic variables such as x_{Bj}, Q^2 and z. Already in the 1970s, SIDIS was understood as a tool to access the intrinsic transverse momentum of the partons (see e.g. [3] and references therein). The connection between the intrinsic transverse momenta of the parton $k_\perp$ and that of the hadron $p_\perp$ and the measured transverse momentum p_T of the produced hadron is illustrated in Fig. 1, assuming single photon exchange and leading order pQCD.

During the last three decades significant efforts, both in experimental and theoretical studies of (polarised) SIDIS, have been undertaken. Currently this process is considered to be one of the most promising to study the spin-dependent three-dimensional structure of the nucleon and also the hadronisation process (see, e.g. [4]). Recently, a complete QCD treatment of transverse momentum and spin-dependent SIDIS was presented in Ref. [5] where factorisation was derived in terms of well defined unintegrated or Transverse Momentum Dependent parton distribution and fragmentation functions (TMDs) with individual hard scale evolution properties. This formalism has been applied in Ref. [6] to obtain the Q^2 evolution of unpolarised TMDs; a mandatory information needed for a correct comparison of data measured in experiments at different hard scales [4].

Hadron leptoproduction has been studied by many experiments. Some recent examples are: JLab [7], HERMES [8] and E665 [9]. Earlier, EMC [10] covered most of the kinematic range of COMPASS. However, COMPASS has collected much more data in this range and the statistical errors of the present analysis are therefore significantly smaller, although only part of the available data has been used. The results presented here are obtained from data taken during the year 2004. More details of the analysis are described in Ref. [11].

2 Experiment, data selection and acceptance

The COMPASS experiment is installed on the M2 beam line of the CERN SPS [12]. Polarised 160 GeV/c muons with an intensity of 2×10^8 μ/spill (one spill of 4.8 s length per 16.8 s) and a polarisation of 80 % are scattered off a longitudinally polarised, isoscalar target that consists of granulated ^{6}LiD immersed in liquid helium. The small admixtures of H, ^{3}He, and ^{7}Li lead to an excess of neutrons of about 0.1 %. In 2004 the target consisted of two cells with opposite polarisation which was reversed every 8 hours. It has been verified that summing up the data from both cells yields a data sample with vanishing polarisation for the present analysis. The COMPASS detector is a large acceptance two-stage spectrometer which covers the kinematic range from quasi-real photoproduction to DIS. Both stages are equipped with hadron calorimeters and use absorber walls for muon identification. Charged particles emerging from the primary interaction vertex in the forward direction are identified as muons if they traverse at least 30 radiation length, otherwise they are identified as hadrons. The selection requires reconstructed trajectories in the detectors situated upstream and downstream of the first magnet. This ensures that the track momentum and sign of charge are well defined by bending in the magnetic field. The COMPASS ability to separate pions, kaons and protons with a Ring Imaging Cherenkov detector was not used in this analysis. Muon interactions with $Q^2 > 1.0$ (GeV/c)^2 and $0.1 < y < 0.9$ are selected, where $y = \nu/E_\mu$, and $\nu = E_\mu - E_{\mu'}$ is the difference between the laboratory energies of the incoming and outgoing muon μ and μ'. With the above selection, the hadronic energy squared $W^2 = 2M\nu + M^2 - Q^2$ is >25 GeV/c, above

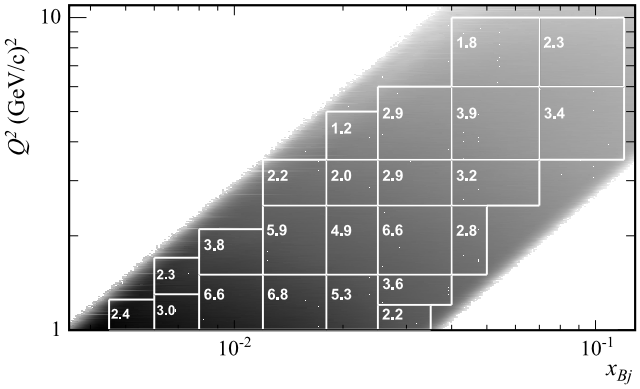

Fig. 2 Event distribution in the 23 bins in the inclusive variables Q^2 and x_{Bj}. Within each bin, the fraction of events contained is indicated in %

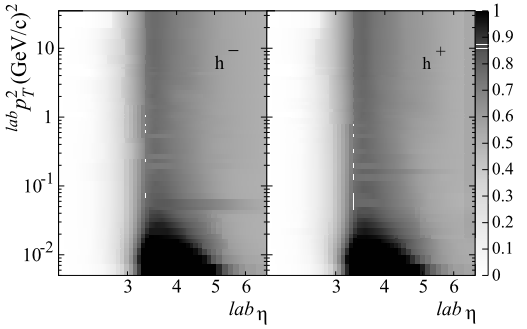

Fig. 3 Hadron acceptances A_{h^-} and A_{h^+} determined with the Monte Carlo simulation for $Q^2 > 1$ (GeV/c)^2 as a function of $^{\text{lab}}p_T$ and $^{\text{lab}}\eta$ for negative hadrons h^- (*left*) and positive hadrons h^+ (*right*). The acceptances have been smoothed in order to reduce the granularity from the binning

the nucleon resonance region. Here, M is the nucleon mass. The total number of inclusive events selected for this analysis is 45.8×10^6, corresponding to an integrated luminosity of 775 pb^{-1}. The events are sampled into 23 intervals in Q^2 from 1 to 10 (GeV/c)^2 and x_{Bj} from 0.004 to 0.12, as shown in Fig. 2. The ranges and average values of Q^2 and x_{Bj} are shown in the Appendix in Table 1. Each of these (x_{Bj}, Q^2) intervals is further subdivided into 8 intervals in z from 0.2 to 0.8. No attempt was made to further suppress diffractive meson production, as done e.g. in Ref. [13].

In order to correct for event losses caused by the non uniform acceptance of the COMPASS spectrometer, a full Monte Carlo (MC) simulation has been performed. The events were generated with LEPTO [14], passed through the spectrometer with a GEANT [15, 16] based simulation program and reconstructed with the reconstruction software as the real data events.

The SIDIS acceptances $A_{\text{SIDIS}}^{(+,-)}$ for detecting, together with the scattered muon, a positive (h^+) or negative hadrons (h^-) respectively factorise in an inclusive muon acceptance $A_{\text{incl}}(Q^2, y)$ and a positive or negative hadron acceptance $A_{h^{(+,-)}}(^{\text{lab}}p_T, ^{\text{lab}}\eta)$. These acceptances depend on the spectrometer characteristics, making the use of variables defined in the laboratory frame preferable; therefore, the transverse momentum $^{\text{lab}}p_T$, the polar angle $^{\text{lab}}\theta$, and the pseudorapidity $^{\text{lab}}\eta = -\ln(\tan\frac{^{\text{lab}}\theta}{2})$ of the hadron are defined with respect to the direction of the incoming muon. The choice of $^{\text{lab}}\theta$ is particularly convenient to exhibit the acceptance cut due to the aperture limit of the polarised target magnet at $^{\text{lab}}\theta = 70$ mrad for the upstream edge of the target. The factorisation of hadron and muon acceptances implies that the differential multiplicities only depend on $A_{h^{(+,-)}}$ since A_{incl} cancels, see Eq. (2). Figure 3 shows the hadron acceptances A_{h^-} and A_{h^+} used in the analysis.

The four-dimensional acceptance used in the present analysis is integrated over the azimuthal angle of the hadrons, i.e. does not take into account the azimuthal modulations in the cross section [2]. The systematic effect on the extracted $\langle p_T^2 \rangle$ have been investigated and found to be negligible.

3 Results

The differential multiplicities $d^2n^{h\pm}/dz\,dp_T^2$ in (Q^2, x_{Bj}) bins are defined in the introduction in terms of the semi-inclusive and inclusive differential cross sections. They are obtained as the acceptance corrected number of hadrons $\Delta^4 N^{h\pm}$ in 8×40 $(z,\ p_T^2)$ bins and 23 $(\Delta x_{Bj}, \Delta Q^2)$ bins, divided by the number $\Delta^2 N^{\mu}$ of muon interactions in the same $(\Delta x_{Bj}, \Delta Q^2)$ bins:

$$\left.\frac{d^2n^{h\pm}(z,\, p_T^2, x_{Bj},\, Q^2)}{dz\,dp_T^2}\right|_{\substack{\Delta x_{Bj} \\ \Delta Q^2}} \approx \frac{\frac{\Delta^4 N^{h\pm}(z, p_T^2, x_{Bj}, Q^2)}{\Delta z \Delta p_T^2 \Delta x_{Bj} \Delta Q^2}}{\frac{\Delta^2 N^{\mu}(x_{Bj}, Q^2)}{\Delta x_{Bj} \Delta Q^2}}. \quad (3)$$

The distributions for two selected $(Q^2,\ x_{Bj})$ bins are shown in Fig. 4 for all z intervals. The full data set, including more p_T^2 bins, is available on HEPDATA [17]. As can be seen from Eq. (3) the uncertainty of the integrated luminosity cancels and the only contributions to systematic uncertainties of the multiplicities come from the hadron acceptance and the assumption of factorisation of hadron and muon acceptance. The total systematic uncertainty due to acceptance has been estimated to be 5 % of the measured multiplicity value [11]. Only statistical errors are shown in the figures.

The fits are performed at values of p_T^2 smaller than 0.72 (GeV/c)^2 to stay away from pQCD effects where the assumption of a simple exponential distribution is known to fail [18, 19] and at p_T^2 larger than 0.01 (GeV/c)^2 to exclude a region where the experimental resolution may affect the distribution. In this range, the p_T^2 distributions are fitted with

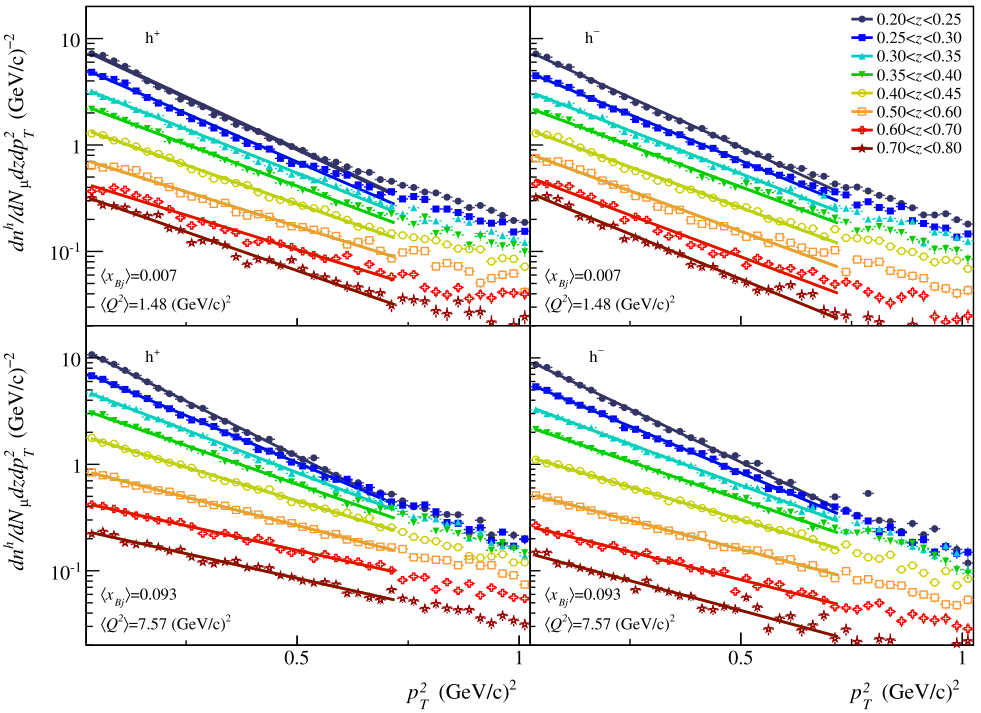

Fig. 4 The p_T^2 dependence of the differential multiplicities $d^2n^h/dz\,dp_T^2$ of positive hadrons (*left*) and negative hadrons (*right*) fitted by an exponential for $1\ (\mathrm{GeV}/c)^2 < Q^2 < 1.5\ (\mathrm{GeV}/c)^2$, $0.006 < x_{Bj} < 0.008$ (*top*) and $6\ (\mathrm{GeV}/c)^2 < Q^2 < 10\ (\mathrm{GeV}/c)^2$, $0.07 < x_{Bj} < 0.12$ (*bottom*) subdivided into eight z intervals, see legend of upper pictures. The average values $\langle Q^2\rangle$ and $\langle x_{Bj}\rangle$ for the chosen (Q^2, x_{Bj}) intervals are indicated in the pictures. The systematic error of 5 % is not included in the errors. The *lines* show the fit result in the fitted range $0.01\ (\mathrm{GeV}/c)^2 < p_T^2 < 0.72\ (\mathrm{GeV}/c)^2$

a single exponential functions $Ae^{-p_T^2/\langle p_T^2\rangle}$ to extract the inverse slope $\langle p_T^2\rangle$. The values of $\langle p_T^2\rangle$ for all intervals of x_{Bj}, Q^2 and z are shown in the Appendix, in Figs. 13 and 14 and in Tables 2 and 3. These figures and tables contain the basic experimental information extracted from the fits of the p_T^2 distributions.

In Fig. 5 the dependence of $\langle p_T^2\rangle$ on x_{Bj} is shown for a low-z and a high-z bin and for a low- and a high-Q^2 bin. At higher z the positive hadrons clearly have higher $\langle p_T^2\rangle$ than the negative hadrons. For hadrons with lower z however, no such difference is observed in the p_T^2 distributions. A similar behaviour was already reported by HERMES [8, 20] for the average p_T^2, not determined by a fit but from a standard average over the entire p_T range, i.e. $\langle p_T^2\rangle_{\mathrm{all}}$. The z-dependence as well as the hadron charge dependence of the p_T^2 distributions will be further investigated below.

It is interesting to compare the values and W^2-dependence of $\langle p_T^2\rangle$ obtained from the fit at small p_T with the values and W^2-dependence of $\langle p_T^2\rangle_{\mathrm{all}}$. The W^2-dependence of $\langle p_T^2\rangle$, obtained from the fit in the bin $0.5 < z < 0.6$ is shown in Fig. 6, that one of $\langle p_T^2\rangle_{\mathrm{all}}$ in Fig. 7. In addition to the data points, Fig. 7 shows lines, which represent fits of the data points assuming a linear function of $\ln W^2$.

The p_T^2 distribution of charged hadrons with $0.5 < z < 0.6$, integrated over Q^2 and x_{Bj}, is shown in Fig. 8(left); this distribution is corrected for acceptance and was used to determine the correct value of $\langle p_T^2\rangle_{\mathrm{all}}$. This quantity is interesting since the authors of Ref. [21] first suggested that $\langle p_T^2\rangle_{\mathrm{all}}$ should depend linearly on the μN center of mass energy squared s, and justified their prediction using results from three fixed target experiments: JLab, HERMES and COMPASS. Fig. 8(right) taken from Ref. [21] shows the $\langle p_T^2\rangle_{all}$ dependence on s. The black dot value for COMPASS was based on previously published data not corrected for acceptance. The current COMPASS value is the red point added to Fig. 8(right). The effect is in any case small.

The current COMPASS point is also shown in a recent paper [22], and was used to quantify the p_T broadening [23] in a model to determine the Sivers and Boer-Mulders asymmetries at COMPASS and HERMES. The result of the model of Ref. [22] is closer to the COMPASS data when p_T broadening is included. The authors of Ref. [21] also note that $\langle p_T^2\rangle_{\mathrm{all}}$ may depend linearly on W^2 rather than s. However, the dependence shown in Fig. 7 is better reproduced by a linear dependence on $\ln W^2$ as was found by EMC [10]. The relation is not well established and, as mentioned in Ref. [21], the linear dependence on s for Drell-Yan muon pair production, which inspired their SIDIS prediction, could also be a linear dependence on $\sqrt{s}$. Contrary to the case of $\langle p_T^2\rangle_{\mathrm{all}}$ in Fig. 7, the W^2-dependence of $\langle p_T^2\rangle$ shown in Fig. 6 is much weaker, as expected, since $\langle p_T^2\rangle$ is assumed to be unaffected by pQCD, as opposed to $\langle p_T^2\rangle_{all}$.

Another interesting observable is the ratio of the multiplicities of positive and negative hadrons integrated over p_T^2 and Q^2. The hadron multiplicity ratios are shown in Fig. 9 as a function of z for different x_{Bj} bins and compared with previous data taken by the EMC experiment [10]. COMPASS results show clearly that the fraction of positive hadrons increases with x_{Bj} (getting closer to the valence region) and z (more related to the energy of the struck parton). This

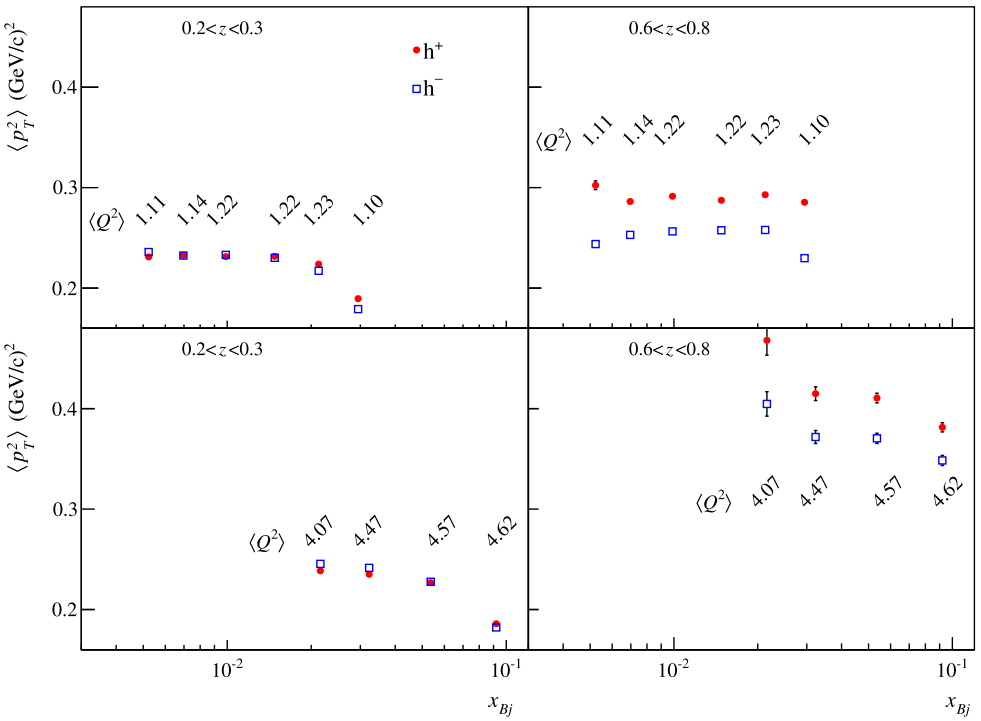

Fig. 5 The fit parameter $\langle p_T^2 \rangle$ obtained in the range $0.01\ (\mathrm{GeV}/c)^2 < p_T^2 < 0.72\ (\mathrm{GeV}/c)^2$ (see Fig. 4) vs x_{Bj} for two different Q^2 intervals (*top* and *bottom*) and for a low-z bin (*left*), and a high-z bin (*right*), for positive and negative hadrons (*red filled circles* and *blue open boxes*). Statistical errors on the fitted $\langle p_T^2 \rangle$ values are also shown. The average value $\langle Q^2 \rangle$ for each x_{Bj} bin is indicated

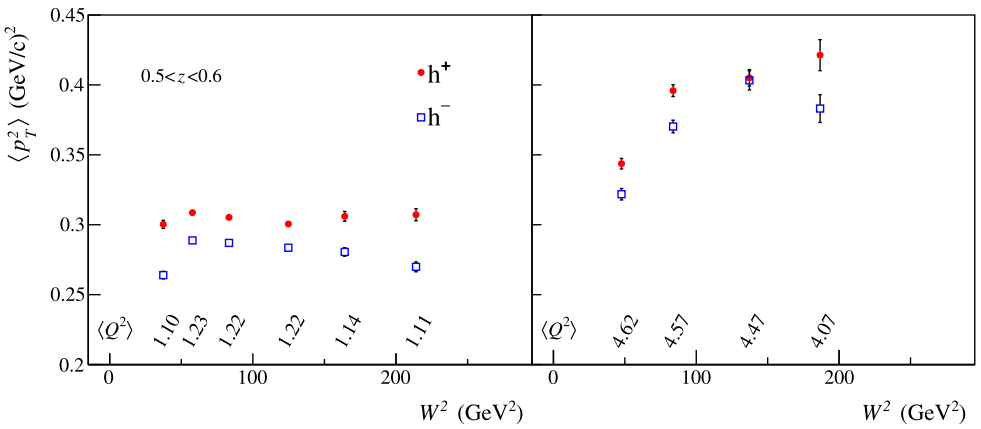

Fig. 6 The fit parameter $\langle p_T^2 \rangle$ obtained in the range $0.01\ (\mathrm{GeV}/c)^2 < p_T^2 < 0.72\ (\mathrm{GeV}/c)^2$ (see Fig. 4) vs W^2 for $0.5 < z < 0.6$ and for a low (*left*) and a high (*right*) Q^2 interval. Statistical errors on the fitted $\langle p_T^2 \rangle$ values are also shown. These results have to be compared with Fig. 7 where $\langle p_T^2 \rangle_{\mathrm{all}}$ is plotted. The average $\langle Q^2 \rangle$ for each W^2 bin are indicated

behaviour is connected with the fact that the positive valence quarks have a larger electric charge than the negative ones. In the valence region, a similar linear behaviour for the deuteron target was also observed for charged pion production at JLab, at much smaller energies [24].

The z^2-dependence of $\langle p_T^2 \rangle$ is of particular interest since it gives a way to access the intrinsic transverse momenta $k_\perp$ and $p_\perp$. At leading order QCD, assuming single photon exchange and an independent fragmentation process, the hadron muoproduction cross section can be expressed in terms of a hard muon-parton interaction cross section convoluted with two unintegrated (transverse momentum dependent) non-perturbative universal functions: the parton distribution function $f_q(x_{Bj}, k_\perp)$ and the fragmentation function $D_q^h(z, p_\perp)$. With the further assumption that both $f_q(x_{Bj}, k_\perp)$ and $D_q^h(z, p_\perp)$ follow a Gaussian distributions with respect to $k_\perp$ and $p_\perp$, respectively, the cross section can be written at first order in $\mathcal{O}(k_\perp/Q)$ by [18]:

$$\frac{d^4\sigma^{\mu N \to \mu' h X}}{dx_{Bj}\,dQ^2\,dz\,dp_T^2} \approx \sum_q \frac{2\pi\alpha^2 e_q^2}{Q^4} f_q(x_{Bj}) D_q^h(z)\left[1+(1-y)^2\right] \times \frac{1}{\langle p_T^2 \rangle_q} e^{-p_T^2/\langle p_T^2 \rangle_q}, \tag{4}$$

where $f_q(x_{Bj})$ and $D_q^h(z)$ are ordinary distribution and fragmentation functions and all the parameters describing the transverse momentum dependence of TMDs for a given

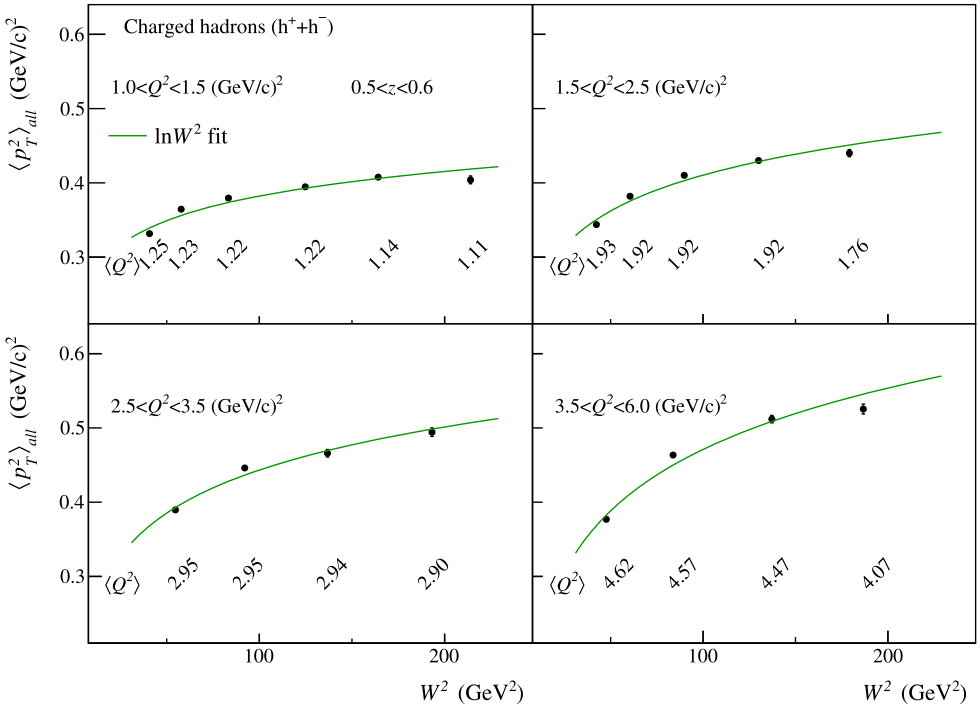

Fig. 7 Average value of the squared transverse momentum $\langle p_T^2 \rangle_{\text{all}}$ over the entire p_T range for charged hadrons (h^+ and h^- summed up) as a function of W^2, for $0.5 < z < 0.6$ and four Q^2 intervals, indicated in the figures. The error on the statistical average is also plotted. The *green lines* represent fits where a linear function of $\ln W^2$ was assumed

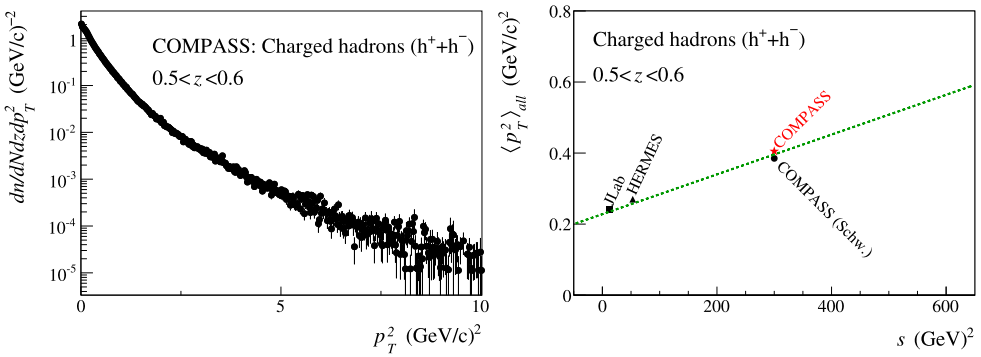

Fig. 8 (*Left*) COMPASS charged hadrons p_T^2 distribution in the range $0.5 < z < 0.6$. (*Right*) Average $\langle p_T^2 \rangle_{all}$ in the range $0.5 < z < 0.6$ for different experiments (JLab, HERMES and COMPASS) as a function of the total energy squared s (*black points*) an the extracted s-dependence from Ref. [21] (*green dotted line*). The *black dot* labelled COMPASS (Schw.) was the value used in Ref. [21], from previously published COMPASS results not corrected for acceptance. The *red star* labelled COMPASS is the current value obtained from the left plot of this figure after applying acceptance correction

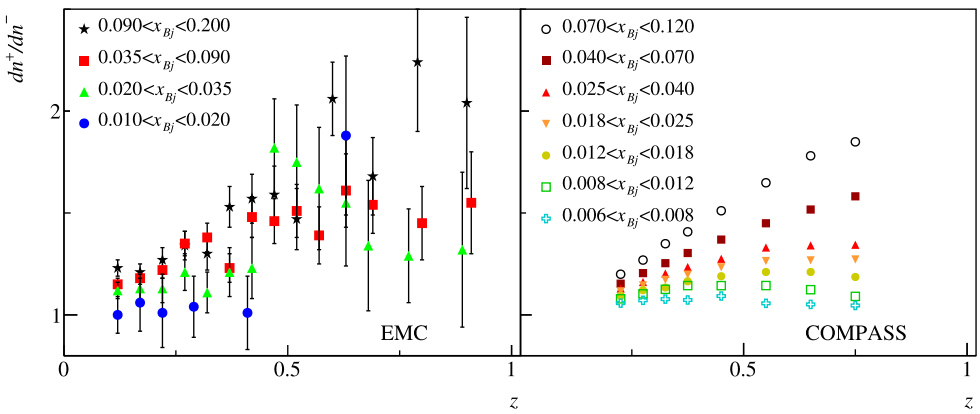

Fig. 9 Charged hadron multiplicity ratios dn^{h+}/dn^{h-} as a function of z, for various x_{Bj} bins, measured by EMC [10] for μd (*left*) and COMPASS for μ^6LiD (*right*) interactions respectively

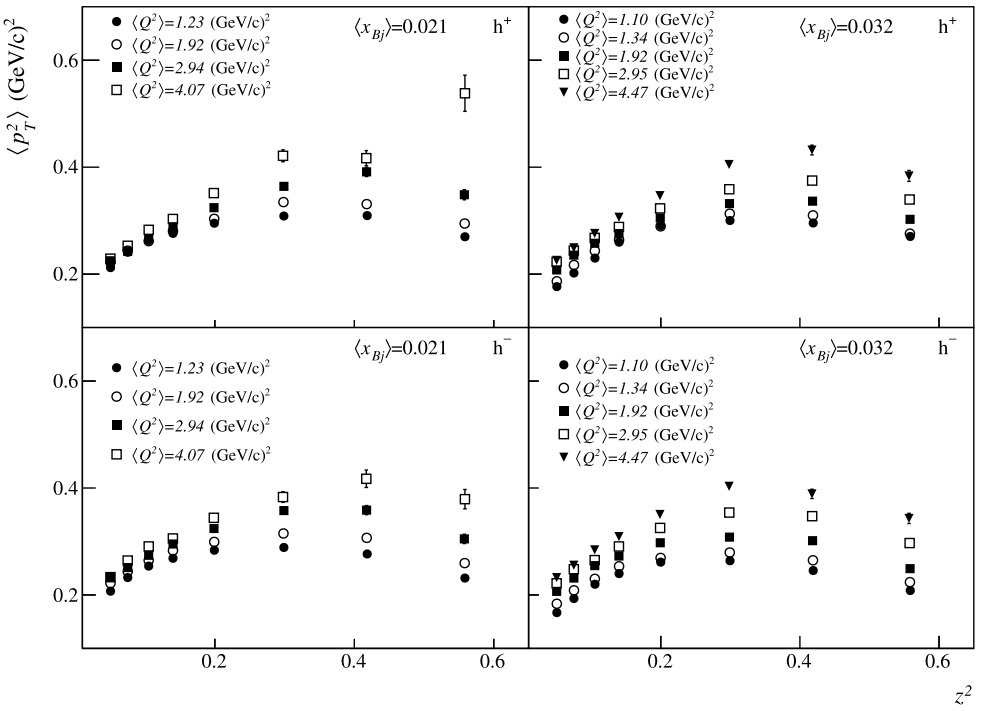

Fig. 10 $\langle p_T^2 \rangle$ vs z^2 for two x_{Bj} intervals and for different Q^2. $\langle p_T^2 \rangle$ becomes larger at fixed x_{Bj} and z with increasing Q^2. The effect is more visible at higher z^2 values where the contribution of the quark intrinsic transverse momentum to the hadron transverse momentum is enhanced

quark flavour q are contained in $\langle p_T^2 \rangle_q$, through the relation:

$$\langle p_T^2 \rangle_q = \langle p_\perp^2 \rangle_q + z^2 \langle k_\perp^2 \rangle_q. \tag{5}$$

Here again, integration over the azimuthal angle has been performed. In Ref. [18] it was assumed that $\langle p_\perp^2 \rangle$ and $\langle k_\perp^2 \rangle$ in Eq. (5) are constants and independent of the quark flavour (this is not the case in a recent analysis of CLAS data [24]). In general, they may both depend on Q^2 and q, while $\langle p_\perp^2 \rangle$ can depend further on z and the produced hadron type, and $\langle k_\perp^2 \rangle$ may depend on x_{Bj}.

One of the most prominent recent achievements in the QCD theory of TMDs is the prediction, see Ref. [6], of broadening of the widths of quark intrinsic transverse momentum distribution and the hadron transverse momentum distribution acquired in fragmentation with increasing Q^2. In Fig. 10 we show the z^2-dependence of $\langle p_T^2 \rangle$ for different Q^2 values in two different x_{Bj} intervals for positive and negative hadrons. As one can see, at fixed x_{Bj} and z values $\langle p_T^2 \rangle$ becomes larger with increasing Q^2. The effect is more visible at higher z^2 values where the contribution of the quark intrinsic transverse momentum to hadron transverse momentum is enhanced, see Eq. (5). The observed Q^2 dependence of $\langle p_T^2 \rangle$ in our data is in qualitative agreement with the predictions of QCD TMD evolution of Ref. [6].

The observed dependence of $\langle p_T^2 \rangle$ on z^2 is shown for two (Q^2, x_{Bj}) intervals in Fig. 11. The relation between $\langle p_T^2 \rangle$ and z^2 is certainly not linear as in Eq. (5). A more general ansatz for the contributions of the intrinsic transverse momenta $p_\perp$ and $k_\perp$ to the measured hadron transverse momentum p_T is

$$\langle p_T^2(z) \rangle = \langle p_\perp^2(z) \rangle + z^2 \langle k_\perp^2 \rangle, \tag{6}$$

where $\langle p_\perp^2(z) \rangle$ is a function of z and should be taken from other measurements. The dependence of $k_\perp$ is still the same as in Eq. (5), with a constant average $\langle k_\perp^2 \rangle$. The knowledge of $\langle p_\perp^2(z) \rangle$ could be taken from DIS event generators which are supposed to incorporate all known properties of jet fragmentation. In Fig. 12 the measured values of $\langle p_T^2 \rangle$ are compared with those of a simulation using the event generator LEPTO.[1] Two cases were simulated in the MC: interactions without intrinsic transverse parton momenta $\langle k_\perp^2 \rangle = 0$ (open squares) and interactions with $\langle k_\perp^2 \rangle = 0.25$ (GeV/c)^2 (open crosses). For $\langle k_\perp^2 \rangle = 0.25$ (GeV/c)^2, the agreement between $\langle p_T^2 \rangle$ from simulated events and from data (full squares) is striking for lower values of Q^2, apart from the highest z^2 bins. For values of Q^2 larger than 4 (GeV/c)^2, the data are significantly above the simulation. The differences between positive and negative hadrons at larger z values are not reproduced by the MC simulation. This comparison suggests that a detailed tuning of the jet fragmentation parameters is needed to extract $\langle k_\perp^2 \rangle$ from the data.

[1] For these simulations, MRST2004LO PDFs in LHAPDF 5.2.2 were used; default LEPTO 6.5.1 and JETSET 7.4 settings, with the exception of LST(11) = 122, which includes target mass effects and the longitudinal structure function.

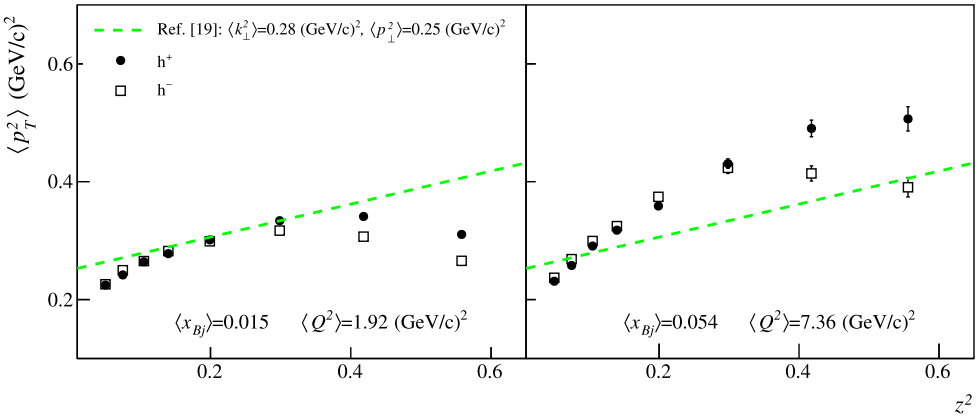

Fig. 11 $\langle p_T^2 \rangle$ vs z^2 for two (Q^2, x_{Bj}) intervals. The corresponding average values $\langle Q^2 \rangle$ (in units of $(\mathrm{GeV}/c)^2$ and $\langle x_{Bj} \rangle$ are indicated in the figure. The *dotted green line* corresponds to relation (5) with constant $\langle k_\perp^2 \rangle$ and $\langle p_\perp^2 \rangle$ from Ref. [19]

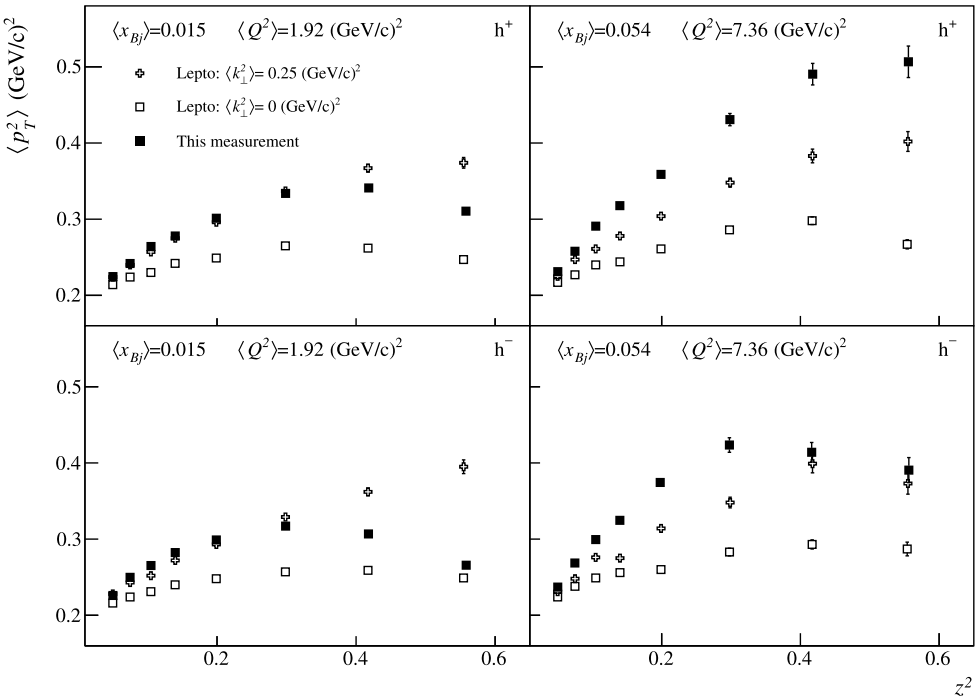

Fig. 12 Comparison of the measured $\langle p_T^2 \rangle$ (*full squares*) with a simulation using the MC event generator LEPTO for two bins of Q^2 and x_{Bj}, for positive (*top*) and negative hadrons (*bottom*). Two cases were simulated in the MC: Interactions without intrinsic transverse parton momenta $\langle k_\perp^2 \rangle = 0$ (*open squares*) and interactions with $\langle k_\perp^2 \rangle = 0.25\ (\mathrm{GeV}/c)^2$ (*open crosses*)

4 Conclusion

The main result of this analysis is the measurement of differential multiplicities of charged hadrons produced in unpolarised SIDIS of muons off an isoscalar target. The acceptance corrected multiplicities in a 4-dimensional (z, p_T^2, x_{Bj}, Q^2) phase space are presented and are available in HepData [17] separately for positively and negatively charged hadrons.

From these distributions other observables have been extracted. The average p_T^2 over the entire p_T range, $\langle p_T^2 \rangle_{\mathrm{all}}$, has been provided for a comparison with other experiments at different center of mass energy. The evolution of $\langle p_T^2 \rangle_{\mathrm{all}}$ as function of the invariant mass W^2 has been found to follow a linear dependence on $\ln W^2$ reasonably well. The ratio of positive to negative hadrons was measured with high precision as a function of z for bins in x_{Bj}. At large x_{Bj} it exhibits a strong rise with increasing z.

The differential distributions at low p_T^2 have been fitted with an exponential in different z bins in order to obtain $\langle p_T^2 \rangle$. The measured $\langle p_T^2 \rangle$ shows complicated dependences on the kinematic variables x_{Bj}, z and Q^2 and on the hadron charge. The observed Q^2 dependences of $\langle p_T^2 \rangle$ in our data at fixed x_{Bj} are in qualitative agreement with the recent predictions of TMD QCD evolution [6]—the broadening of transverse momentum distribution in TMD DFs and FFs as the hard scale increases. The assumptions of Ref. [18] of $\langle k_\perp^2 \rangle$ and $\langle p_\perp^2 \rangle$ being constants is not adequate to describe correctly the new and precise COMPASS data.

A new global multidimensional analysis of multiplicities is needed to extract $\langle k_\perp^2 \rangle$ and $\langle p_\perp^2 \rangle$. This analysis was not performed in the past due to the lack of data. The high statistics multidimensional results from COMPASS presented in this paper will provide a starting point, while a dedicated study of the hadron transverse momentum distribution in e^+e^- annihilation, to which only $p_\perp$ contributes, will be another important input to this analysis.

Another possible way to access the intrinsic transverse momentum $\langle k_\perp^2 \rangle$ is by tuning of the Monte Carlo generator such that it describes the multiplicity data. Also in this case, the already mentioned dependence of the generated $k_\perp$ on kinematic variables needs to be implemented in the generator.

This is the first multidimensional study of hadron multiplicities in unpolarised SIDIS at COMPASS. Further analyses, using the COMPASS ability to identify hadrons, are under way to investigate the production of charged pions and kaons.

Acknowledgement We gratefully acknowledge the support of the CERN management and staff and the skill and effort of the technicians of our collaborating institutes. Special thanks go to V. Anosov and V. Pesaro for their technical support during the installation and the running of this experiment. This work was made possible by the financial support of our funding agencies.

Appendix

Table 1 Definition of the 23 bins of x_{Bj} and Q^2 and corresponding mean values; Q^2 is in units of $(\mathrm{GeV}/c)^2$

Bin	$x_{Bj}^{\min}$	$x_{Bj}^{\max}$	$\langle x_{Bj} \rangle$	$Q^2_{\min}$	$Q^2_{\max}$	$\langle Q^2 \rangle$
1	0.0045	0.0060	0.0052	1.0	1.25	1.11
2	0.0060	0.0080	0.0070	1.0	1.30	1.14
3	0.0060	0.0080	0.0070	1.3	1.70	1.48
4	0.0080	0.0120	0.0099	1.0	1.50	1.22
5	0.0080	0.0120	0.0099	1.5	2.10	1.76
6	0.0120	0.0180	0.0148	1.0	1.50	1.22
7	0.0120	0.0180	0.0148	1.5	2.50	1.92
8	0.0120	0.0180	0.0150	2.5	3.50	2.90
9	0.0180	0.0250	0.0213	1.0	1.50	1.23
10	0.0180	0.0250	0.0213	1.5	2.50	1.92
11	0.0180	0.0250	0.0213	2.5	3.50	2.94
12	0.0180	0.0250	0.0216	3.5	5.00	4.07
13	0.0250	0.0350	0.0295	1.0	1.20	1.10
14	0.0250	0.0400	0.0316	1.2	1.50	1.34
15	0.0250	0.0400	0.0318	1.5	2.50	1.92
16	0.0250	0.0400	0.0319	2.5	3.50	2.95
17	0.0250	0.0400	0.0323	3.5	6.00	4.47
18	0.0400	0.0500	0.0447	1.5	2.50	1.93
19	0.0400	0.0700	0.0533	2.5	3.50	2.95
20	0.0400	0.0700	0.0536	3.5	6.00	4.57
21	0.0400	0.0700	0.0550	6.0	10.0	7.36
22	0.0700	0.1200	0.0921	3.5	6.00	4.62
23	0.0700	0.1200	0.0932	6.0	10.0	7.57

Table 2 Fitted $\langle p_T^2 \rangle$ in units of $(\mathrm{GeV}/c)^2$ for the 23 $(x_{Bj},\ Q^2)$ bins (rows) and the 8 z intervals (columns) for positive hadrons. The error of the least significant digit(s) is given in parentheses. Same information as Fig. 13

Q^2, x_{Bj} Bin	z bins							
	0.2÷0.25	0.25÷0.3	0.3÷0.35	0.35÷0.4	0.4÷0.5	0.5÷0.6	0.6÷0.7	0.7÷0.8
1	.2254(13)	.2394(17)	.2607(23)	.2738(30)	.2981(31)	.3072(43)	.3299(65)	.2674(57)
2	.2241(10)	.2457(14)	.2614(19)	.2763(24)	.2952(24)	.3060(35)	.3009(44)	.2650(46)
3	.2234(13)	.2390(18)	.2631(24)	.2761(31)	.2986(32)	.3327(52)	.3348(69)	.2985(68)
4	.2239(6)	.2424(9)	.2592(12)	.2738(15)	.2915(15)	.3006(21)	.3087(29)	.2670(30)
5	.2270(9)	.2438(13)	.2634(17)	.2777(22)	.3073(24)	.3387(38)	.3419(51)	.2998(55)
6	.2231(6)	.2442(8)	.2610(11)	.2755(14)	.2914(13)	.3053(19)	.3010(25)	.2677(27)
7	.2246(7)	.2418(9)	.2641(13)	.2779(17)	.3013(17)	.3338(27)	.3410(38)	.3105(44)
8	.2250(13)	.2470(18)	.2723(25)	.2893(33)	.3338(38)	.3829(67)	.420(11)	.447(17)
9	.2122(7)	.2408(9)	.2630(12)	.2762(15)	.2953(15)	.3087(21)	.3094(26)	.2699(27)
10	.2222(7)	.2439(10)	.2617(13)	.2806(17)	.3034(17)	.3347(28)	.3309(37)	.2946(39)
11	.2250(12)	.2425(16)	.2667(22)	.2886(30)	.3243(34)	.3642(57)	.3912(88)	.3485(95)
12	.2289(17)	.2530(24)	.2828(35)	.3031(48)	.3515(55)	.421(11)	.417(14)	.538(34)
13	.1766(13)	.2020(15)	.2299(18)	.2597(23)	.2909(22)	.3003(29)	.2956(34)	.2704(37)
14	.1866(9)	.2171(13)	.2436(15)	.2640(18)	.2893(17)	.3131(24)	.3099(30)	.2758(31)
15	.2078(6)	.2355(8)	.2577(11)	.2759(14)	.3050(14)	.3319(22)	.3364(29)	.3025(31)
16	.2229(9)	.2441(13)	.2678(18)	.2882(23)	.3230(26)	.3587(42)	.3749(59)	.3395(69)
17	.2257(10)	.2493(14)	.2761(20)	.3064(28)	.3468(32)	.4050(59)	.4321(91)	.384(10)
18	.1799(11)	.2063(13)	.2340(17)	.2500(19)	.2853(20)	.3197(30)	.3321(40)	.2984(42)
19	.1944(9)	.2245(12)	.2486(15)	.2735(20)	.3088(22)	.3434(34)	.3656(49)	.3609(62)
20	.2167(8)	.2415(11)	.2700(15)	.2947(21)	.3370(23)	.3959(42)	.4170(63)	.3994(76)
21	.2311(13)	.2579(18)	.2908(27)	.3178(37)	.3588(41)	.4307(80)	.490(14)	.507(21)
22	.1738(10)	.1990(12)	.2319(16)	.2578(21)	.2969(22)	.3437(38)	.3809(57)	.3809(74)
23	.2091(10)	.2448(15)	.2714(21)	.2989(28)	.3441(31)	.4072(57)	.470(10)	.469(13)

Table 3 Fitted $\langle p_T^2 \rangle$ in units of $(\mathrm{GeV}/c)^2$ for the 23 $(x_{Bj},\ Q^2)$ bins (rows) and the 8 z intervals (columns) for negative hadrons. The error of the least significant digit(s) is given in parentheses. Same information as Fig. 14

Bin	0.2÷0.25	0.25÷0.3	0.3÷0.35	0.35÷0.4	0.4÷0.5	0.5÷0.6	0.6÷0.7	0.7÷0.8
1	.2285(13)	.2472(18)	.2606(24)	.2651(29)	.2741(27)	.2699(35)	.2551(41)	.2259(42)
2	.2241(10)	.2450(15)	.2607(20)	.2713(25)	.2793(23)	.2806(31)	.2697(37)	.2297(37)
3	.2305(14)	.2510(19)	.2690(25)	.2802(33)	.2843(30)	.2851(40)	.2778(50)	.2562(54)
4	.2254(7)	.2448(9)	.2614(13)	.2719(16)	.2814(15)	.2836(20)	.2700(24)	.2375(26)
5	.2276(10)	.2498(14)	.2666(19)	.2752(23)	.2987(24)	.3056(33)	.2990(42)	.2722(46)
6	.2216(7)	.2431(9)	.2604(12)	.2766(15)	.2869(14)	.2870(19)	.2780(24)	.2297(23)
7	.2260(7)	.2498(10)	.2653(14)	.2823(18)	.2989(18)	.3171(27)	.3068(35)	.2657(37)
8	.2346(14)	.2555(19)	.2841(28)	.2976(36)	.3233(38)	.3572(62)	.3674(88)	.328(10)
9	.2071(8)	.2326(10)	.2540(13)	.2686(16)	.2837(15)	.2888(20)	.2767(24)	.2316(24)
10	.2219(8)	.2440(11)	.2646(14)	.2831(19)	.2992(19)	.3150(28)	.3068(36)	.2596(35)
11	.2331(13)	.2512(18)	.2742(25)	.2953(34)	.3243(37)	.3578(62)	.3587(85)	.3048(87)
12	.2333(18)	.2644(27)	.2908(40)	.3057(50)	.3443(58)	.383(10)	.417(16)	.379(18)
13	.1669(12)	.1933(16)	.2201(20)	.2400(23)	.2614(21)	.2640(27)	.2457(29)	.2083(28)
14	.1835(11)	.2086(12)	.2302(15)	.2536(19)	.2693(18)	.2794(24)	.2648(27)	.2240(26)
15	.2067(7)	.2316(9)	.2548(12)	.2728(15)	.2976(16)	.3081(22)	.3015(27)	.2492(26)
16	.2219(10)	.2482(14)	.2652(19)	.2907(26)	.3254(29)	.3541(47)	.3473(62)	.2971(60)
17	.2325(11)	.2556(16)	.2844(23)	.3092(31)	.3506(37)	.4033(68)	.3890(87)	.3432(95)
18	.1746(11)	.1994(14)	.2232(18)	.2411(21)	.2692(21)	.2850(30)	.2882(38)	.2394(35)
19	.1915(9)	.2193(13)	.2452(18)	.2715(23)	.3040(25)	.3268(39)	.3319(51)	.2869(52)
20	.2163(9)	.2456(12)	.2765(18)	.3007(25)	.3389(28)	.3703(45)	.3909(70)	.3382(73)
21	.2370(14)	.2686(21)	.2994(31)	.3246(44)	.3744(53)	.4235(96)	.414(13)	.391(17)
22	.1730(10)	.1967(13)	.2314(19)	.2623(27)	.2867(26)	.3218(41)	.3598(66)	.3310(75)
23	.2166(13)	.2482(17)	.2814(25)	.3050(35)	.3531(41)	.3976(71)	.414(11)	.388(13)

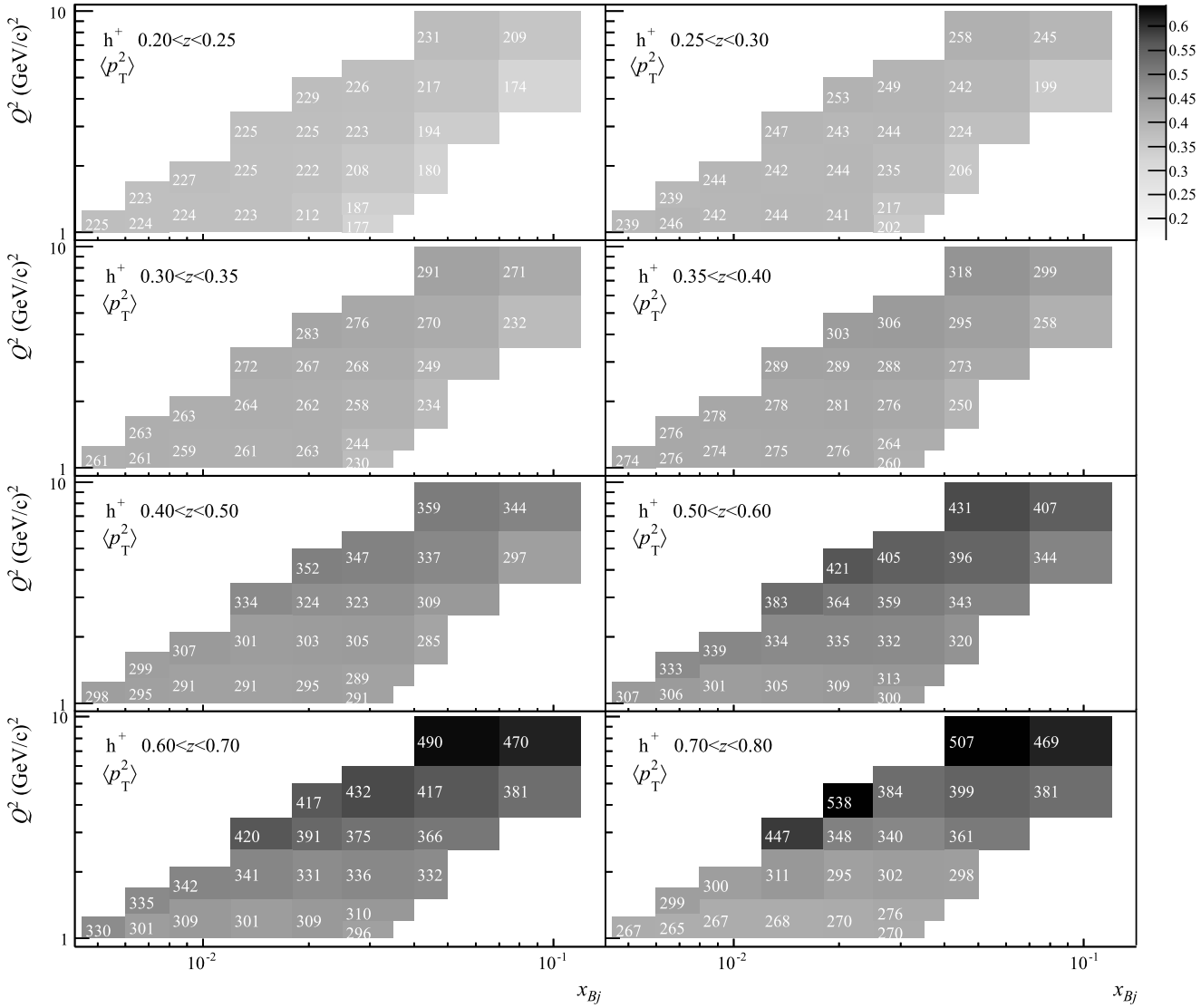

Fig. 13 Fitted $\langle p_T^2 \rangle$ vs (x_{Bj}, Q^2) for all z intervals for positive hadrons. The values are both written inside each interval and shown as a *gray scale*. The same *gray scale* is used for all the plots. The written values are in units of $(\mathrm{GeV}/c)^2 \times 1000$

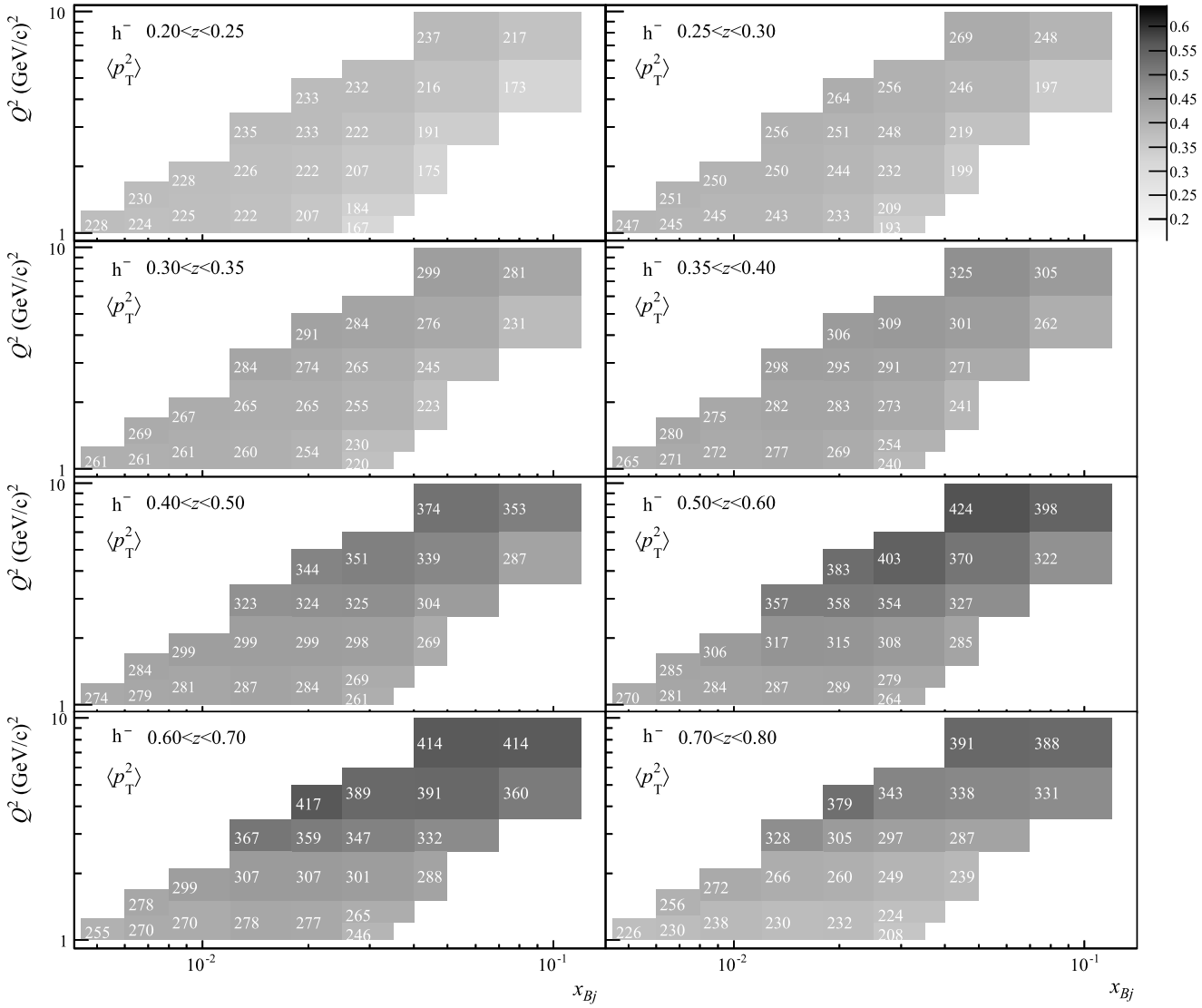

Fig. 14 As Fig. 13 but for negative hadrons

References

1. M. Diehl, S. Sapeta, Eur. Phys. J. C **41**, 515 (2005). arXiv:hep-ph/0503023. doi:10.1140/epjc/s2005-02242-9
2. A. Bacchetta et al., J. High Energy Phys. **0702**, 93 (2007). arXiv:hep-ph/0611265. doi:10.1088/1126-6708/2007/02/093
3. R.N. Cahn, Phys. Lett. B **78**, 269 (1978). doi:10.1016/0370-2693(78)90020-5
4. V. Barone, F. Bradamante, A. Martin, Prog. Part. Nucl. Phys. **65**, 267 (2010). arXiv:1011.0909 [hep-ph]. doi:10.1016/j.ppnp.2010.07.003
5. J.C. Collins, *Foundation of Perturbative QCD* (Cambridge University Press, Cambridge, 2011)
6. S.M. Aybat, T.C. Rogers, Phys. Rev. D **83**, 114042 (2011). arXiv:1101.5057 [hep-ph]. doi:10.1103/PhysRevD.83.114042
7. M. Osipenko et al. (The CLAS Collaboration), Phys. Rev. D **80**, 032004 (2009). arXiv:0809.1153 [hep-ex]. doi:10.1103/PhysRevD.80.032004
8. A. Airapetian et al. (The HERMES Collaboration), Phys. Lett. B **684**, 114 (2010). arXiv:0906.2478 [hep-ex]. doi:10.1016/j.physletb.2010.01.020
9. M.R. Adams et al. (The E665 Collaboration), Z. Phys. C **76**, 441 (1997). doi:10.1007/s002880050567
10. J. Ashman et al. (The EMC Collaboration), Z. Phys. C **52**, 361 (1991). doi:10.1007/BF01412322
11. J.-F. Rajotte, PhD Thesis at Ludwig Maximilian University Munich (2010)
12. P. Abbon et al. (The COMPASS Collaboration), Nucl. Instrum. Methods A **577**, 455 (2007). arXiv:hep-ex/0703049. doi:10.1016/j.nima.2007.03.026
13. A. Airapetian et al. (The HERMES Collaboration), Phys. Rev. D **87**, 074029 (2013). arXiv:1204.4161 [hep-ex]. doi:10.1103/PhysRevD.87.012010
14. G. Ingelman, A. Edin, J. Rathsman, Comput. Phys. Commun. **101**, 108 (1997). arXiv:hep-ph/9605286. doi:10.1016/S0010-4655(96)00157-9
15. S. Agostinelli et al. (GEANT4 Collaboration), Nucl. Instrum. Methods A **506**, 250 (2003). doi:10.1016/S0168-9002(03)01368-8
16. J. Allison et al., IEEE Trans. Nucl. Sci. **53**, 270 (2006). doi:10.1109/TNS.2006.869826
17. The Durham HepData Project. http://hepdata.cedar.ac.uk/reaction
18. M. Anselmino et al., Phys. Rev. D **71**, 074006 (2005). arXiv:hep-ph/0501196. doi:10.1103/PhysRevD.71.074006
19. M. Anselmino, M. Boglione, A. Prokudin, C. Turk, Eur. Phys. J. A **31**, 373 (2007). arXiv:hep-ph/0606286. doi:10.1140/epja/i2007-10003-9
20. A. Jgoun on behalf of the HERMES collaboration, Talk given at 36th Rencontres de Moriond on QCD and Hadronic Interactions (2001)
21. P. Schweitzer, T. Teckentrup, A. Metz, Phys. Rev. D **81**, 094019 (2010). arXiv:1003.2190 [hep-ph]. doi:10.1103/PhysRevD.81.094019
22. B. Pasquini, P. Schweitzer, Phys. Rev. D **83**, 114044 (2011). arXiv:1103.5977 [hep-ph]. doi:10.1103/PhysRevD.83.114044
23. J.C. Collins, D.E. Soper, G. Sterman, Nucl. Phys. B **250**, 199 (1985). doi:10.1016/0550-3213(85)90479-1
24. R. Asaturyan et al., Phys. Rev. C **85**, 015202 (2012). arXiv:1103.1649 [nucl-ex]. doi:10.1103/PhysRevC.85.015202